Available online at www.sciencedirect.com
ScienceDirect
Trans. Nonferrous Met. Soc. China 24(2014) 3413−3420
Transactions of Nonferrous Metals Society of China
www.tnmsc.cn

Influence of cooling rate on solidification behavior of sand-cast Mg−10Gd−3Y−0.4Zr alloy

Song PANG[1,2], Guo-hua WU[1], Wen-cai LIU[1], Liang ZHANG[1], Yang ZHANG[1], Hans CONRAD[2], Wen-jiang DING[1]

1. National Engineering Research Center of Light Alloy Net Forming and State Key Laboratory of Metal Matrix Composite, Shanghai Jiao Tong University, Shanghai 200240, China;
2. Materials Science and Engineering Department, North Carolina State University, Raleigh, NC 27695-7907, USA

Received 30 December 2013; accepted 30 April 2014

Abstract: The effect of the cooling rate ranging from 1.4 °C/s to 3.5 °C/s on the solidification behavior of the sand-cast Mg−10Gd−3Y−0.4Zr alloy was studied by computer aided cooling curve analysis (CA-CCA). With the increase in cooling rate, the nucleation temperature ($T_{\alpha,N}$) increases from 634.8 °C to 636.3 °C, the minimum temperature ($T_{\alpha,Min}$) decreases from 631.9 °C to 630.7 °C, the nucleation undercooling (ΔT_N) increases from 2.9 °C to 5.6 °C, the beginning temperature of the eutectic reaction ($T_{eut,N}$) increases, the time of the eutectic reaction shortens, solidus temperature decreases from 546.0 °C to 541.4 °C, and solidification temperature range (ΔT_S) increases by 6.1 °C. The increased nucleation rate ($\dot{N}$) is supposed to be the main reason for the increased ΔT_N. Increased value ($T_{eut,N}-T_{eut,G}$) and shortened time of the eutectic reaction cause the change in the volume fraction and morphology of the second phase.

Key words: Mg−10Gd−3Y−0.4Zr; sand-cast; cooling rate; thermal analysis; solidification behavior

1 Introduction

The replacement of high density cast iron and steel materials by Mg alloys is of interest in the last few decades, especially in the automotive and the aerospace industries. In recent years, the developing Mg−10Gd−3Y−0.4Zr (GW103K) alloy shows higher specific strength at room and elevated temperatures [1,2], greater creep resistance, and better corrosion resistance compared with the conventional aluminum and other magnesium alloys [3−15].

Most studied GW103K alloys in the research works above were formed through permanent mold in the lab [10]. However, it was reported that the GW103K alloy was used in components with a complex geometry (e.g., transmission housings, engine blocks, etc) which is usually formed by the sand-cast method [13−15]. The cooling rate is one of the most fundamental parameters in the sand-cast process [16,17]. In the modern casting industry, computer aided cooling curve thermal analysis (CA-CCA) of alloys was employed more and more extensively for the evaluation of several processing and material parameters [18]. It provides information on the composition of the alloy, the latent heat of solidification [19], the evolution of fraction solid [20], the types of phases that solidify and even dendrite coherency [21]. It can also be used for determining dendrite arm spacing, degree of modification and grain refinement, and characteristic temperatures related to phase transformation [22,23].

With the consideration of its industrial application and the direct influence on mechanical properties, the aim of this work is to investigate the effects and on-line prediction of cooling rate on microstructure refinement of the sand-cast Mg−10Gd−3Y−0.4Zr (GW103K) alloy using computer aided cooling curve analysis. The results of thermal analysis were used to develop a simple mathematical model which can be used to predict microstructure refinement and phase modification of the cooling rate affected sand-cast GW103K alloy. The mechanism of the grain refinement and the relationships between the modified microstructure and solidification parameters of the eutectic phase caused by the increase

Foundation item: Project (51275295) supported by the National Natural Science Foundation of China; Project (USCAST2012-15) supported by the SAST-SJTU Joint Research Centre of Advanced Aerospace Technology, China; Projects (20120073120011, 20130073110052) supported by the Research Fund for the Doctoral Program of Higher Education of China
Corresponding author: Guo-hua WU; Tel: +86-21-54742630; Fax: +86-21-34202794; E-mail: ghwu@sjtu.edu.cn
DOI: 10.1016/S1003-6326(14)63484-1

in cooling rate were also discussed.

2 Experimental

High purity Mg ingots (99.95%, mass fraction), and Mg−25%Gd, Mg−25%Y and Mg−30%Zr master alloys were used. The melting process was carried out in an electric resistance furnace under the mixed atmosphere of CO_2 and SF_6 with the volume ratio of 100:1. After being refined at 750 °C, the alloy melt was firstly held at 780 °C for 10 min, then cooled to 750 °C and poured into the sand mold. The casting had five mutative cavities with respective thickness (δ) of 5, 10, 15, 20 and 30 mm, as shown in Fig. 1. The chemical composition of the sand-cast alloy was measured by an inductively coupled plasma analyzer (Perkin Elmer, Plasma-400), and the results are listed in Table 1.

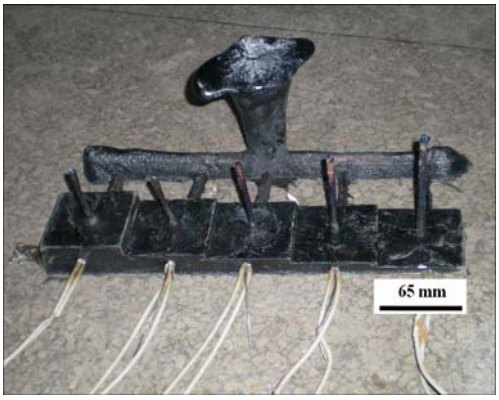

Fig. 1 Photo of casting and location of K-type thermocouples

Table 1 Chemical compositions of sand-cast GW103K alloys

δ/mm	Mass fraction/%			
	Gd	Y	Zr	Mg
30	10.12	3.06	0.42	Bal.
20	10.48	3.12	0.43	Bal.
15	10.22	3.07	0.44	Bal.
10	10.46	3.19	0.43	Bal.

Thermal test was performed in the five-step sand mold by attaching a high sensitivity K-type thermocouple (d=0.3 mm) at the central location of each part, as shown in Fig. 1. To obtain reproducible results, the thermocouples were placed exactly at the centre of each step, with their heads connected through spot welding and the rest insulated with a shield. The data were acquired using a high-speed data acquisition system, linked to a computer through a converter (RS232/485). The signal was recorded each 0.5 s for all data points. The cooling curve data were processed using a thermal analysis program. The processing included smoothing, curve fitting, plotting the first derivatives, identifying the onset and end of solidification, determining solidification parameters such as cooling rate, nucleation temperatures, nucleation undercooling, growth temperature and total solidification time [24]. The first derivative of the cooling curve (dT/dt) was determined to enhance slope changes which were related to the solidification reactions for different phases, and to facilitate the determination of the critical solidification characteristics of the alloys. Details of the cooling process and related solidification parameters are shown in Fig. 2 and Table 2. The cooling rate in the present work was determined using $R_C=(T_{liq}-T_{sol})/(t_{liq}-t_{sol})$, where T_{liq} and T_{sol} are the liquidus and solidus temperatures (°C), and t_{liq} and t_{sol} are the time from the cooling curve that corresponds to liquidus and solidus temperatures, respectively [25]. The grain size was measured using the linear intercept technique (ASTM 112-96). Five fields were considered for each measurement with approximately 60 intercepts in each

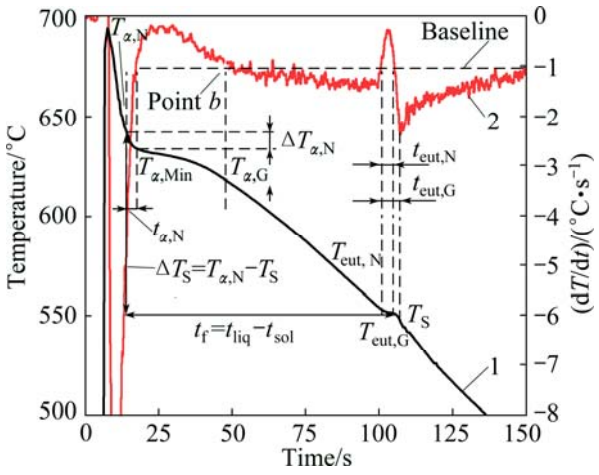

Fig. 2 Cooling curve (line 1), first derivative curve (line 2) and representation of characteristic parameters used in present work for sand-cast GW103K alloy

Table 2 Solidification characteristic parameters shown in Fig. 2

Characteristic symbol	Characteristic description
$T_{\alpha,N}$	α-Mg nucleation (liquidus) temperature
$T_{\alpha,Min}$	α-Mg minimum temperature
ΔT_N	Nucleation undercooling ($\Delta T_N= T_{\alpha,N} -T_{\alpha,Min}$)
$t_{\alpha,N}$	Nucleation time
$T_{\alpha,G}$	α-Mg dendrite growth temperature
$T_{eut,N}$	Eutectic nucleation temperature
$T_{eut,G}$	Eutectic growth temperature
$t_{eut,N}$	Eutectic nucleation undercooling time
$t_{eut,G}$	Eutectic growth time
T_S	Solidus temperature (end of solidification process)
ΔT_S	Solidification temperature range ($\Delta T_S=T_{\alpha,N}-T_S$)
t_f	Total solidification time

field depending on the grain size. The volume fraction of second phase was determined by an image analyzer on optical metallographic sections.

3 Results and discussion

3.1 Cooling curves and summaries of solidification characteristic parameters

Figure 3 shows five cooling curves of sand-cast GW103K alloys at different cooling rates. There are two well-defined stages in each cooling curve, which respectively correspond to the following two reactions during the solidification process of sand-cast GW103K alloys: 1) Nucleation and growth of the primary α-Mg phase; 2) Nucleation and growth of Mg-$Mg_{24}RE_5$ eutectic compound.

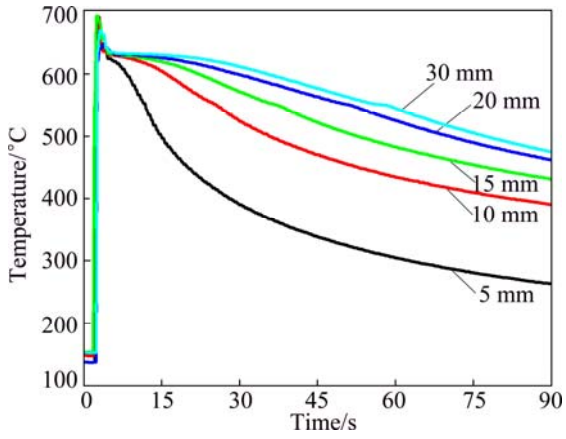

Fig. 3 Cooling curves of sand-cast GW103K alloy at five different thicknesses of casting which related to different cooling rates

Both of those two reactions were brought forward by the increased cooling rate. It is also observed that the liquidus peak disappears gradually with the increase in cooling rate, as shown in Fig. 3. Main solidification parameters calculated from cooling curves at different cooling rates are listed in Table 3. The other solidification parameters are listed in Table 4, which are related to the eutectic reaction.

3.2 Microstructure

Our previous work showed that the influence of the cooling rate on the microstructure of the sand-cast GW103K alloy [15] can be summarized as: 1) The microstructure of sand-cast GW103K alloys consists of the equiaxed α-Mg matrix and the eutectic compound at the grain boundaries; 2) The increase in cooling rate causes the eutectic compound to exhibit continuous network instead of coarsening discontinuous network of plate-shaped microstructure; 3) The average α-Mg grain size decreases from 59 μm to 41 μm, and the volume fraction of the second phase increases from 17.6% to 22.0%, when the cooling rate increases from 1.4 °C/s to 3.5 °C/s.

3.3 Solidification parameters of α-Mg phase

Figure 4 shows the influence of cooling rate (R_C) on the solidification parameters of the α-Mg phase, which include the nucleation temperature ($T_{\alpha,N}$), minimum temperature ($T_{\alpha,Min}$) and growth temperature ($T_{\alpha,G}$) of α-Mg phase. $T_{\alpha,N}$ is the temperature corresponding to the beginning of the liquidus peak on the first derivative curve, which also indicates the start of the solidification. $T_{\alpha,N}$ increases from 634.8 °C to 636.3 °C with the cooling rate increasing from 1.4 °C/s to 3.5 °C/s. It indicates that the higher cooling rate causes an earlier beginning of the nucleation process. Before the nucleation starts, there are embryos in the melt caused by the undercooling which can enhance the driving force for the nucleation [26]. In the present work, high cooling rate leads to high undercooling, which increases the amount of embryos. As a result, the nucleation temperature ($T_{\alpha,N}$) increases, which is due to the increased driving force. There exists a well linear relationship between $T_{\alpha,N}$ and R_C. The empirical fitting function is

$$T_{\alpha,N}=633.87+0.701R_C,\ R^2=0.995 \quad (1)$$

$T_{\alpha,Min}$ is the temperature dividing the main nucleation process from the main growth process of α-Mg phase, which means that most nucleation occurs before this temperature. $T_{\alpha,Min}$ decreases from 631.9 °C to 630.7 °C with the increase in cooling rate. This indicates that the high cooling rate delays the end of the nucleation stage directly, which is the beginning of the growth of the α-Mg phase. This phenomenon implies that the increased cooling rate extends the nucleation process slightly. There exists a well linear relationship between $T_{\alpha,Min}$ and R_C. The empirical fitting function is

Table 3 Characteristic parameters of α-Mg phase and solidification process from cooling curves at different cooling rates

δ/mm	R_C/(°C·s^{-1})	$T_{\alpha,N}$/°C	$T_{\alpha,G}$/°C	$T_{\alpha,Min}$/°C	$\Delta T_{\alpha,N}$/°C	$t_{\alpha,N}$/s	T_S/°C	ΔT_S/°C	t_f/s
30	1.4	634.8	631.5	631.9	2.9	4.75	546.0	88.8	61.2
20	1.6	635.0	631.3	631.7	3.3	3.49	545.6	89.4	57.5
15	2.1	635.4	631.0	631.4	4.0	2.46	544.2	91.2	47.8
10	3.5	636.3	629.7	630.7	5.6	2.29	541.4	94.9	26.6

Cooling curve of the location with thickness δ=5 mm was too rough to be identified.

Table 4 Characteristic parameters of eutectic phases from cooling curves at different cooling rates

δ/mm	R_C/(°C·s^{-1})	$T_{eut,N}$/°C	$T_{eut,G}$/°C	$t_{eut,N}$/s	$t_{eut,G}$/s
30	1.4	557.0	549.7	5.2	2.3
20	1.6	557.6	549.3	2.9	1.6
15	2.1	558.3	548.3	2.6	1.2
10	3.5	559.6	546.3	1.9	1.1

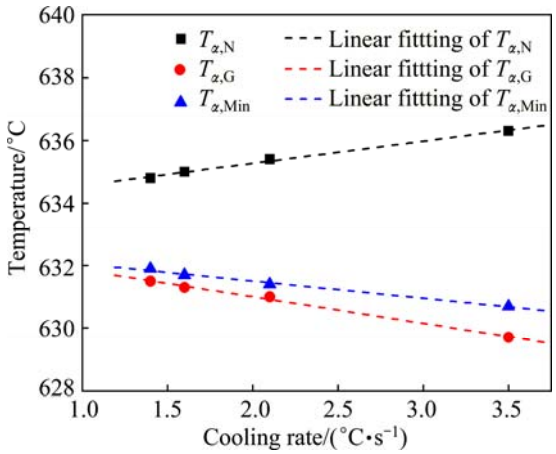

Fig. 4 Relationship between solidification parameters of α-Mg phase ($T_{\alpha,N}$, $T_{\alpha,Min}$ and $T_{\alpha,G}$) and cooling rate

$$T_{\alpha,Min}=632.61-0.552R_C,\ R^2=0.991 \quad (2)$$

$T_{\alpha,G}$ is the temperature corresponding to the end of the α-Mg phase formation, which means that the growth process endures without nucleation of the α-Mg phase. It should be noted that $T_{\alpha,G}$ is lower than $T_{\alpha,Min}$. Similar results were shown in Refs. [19,26−28], which pointed out that the grain refiner played a main role in this kind of behaviour. $T_{\alpha,G}$ decreases from 631.5 °C to 629.7 °C with the increase in cooling rate. This indicates that the increase in cooling rate also delays the total nucleation time by extending the nucleation stage of the α-Mg phase. There also exists a well linear relationship between $T_{\alpha,G}$ and R_C. The empirical fitting function is

$$T_{\alpha,G}=632.71-0.853R_C,\ R^2=0.995 \quad (3)$$

3.4 Undercooling and latent heat of α-Mg phase

Figure 5 shows the relationship between the nucleation undercooling parameters (ΔT_N and Δt_N) of the α-Mg phase and the cooling rate. The nucleation undercooling (ΔT_N) is an effective way to estimate the nucleation activity of the melt, and Δt_N expresses the nucleation process. When the cooling rate increases from 1.4 °C/s to 3.5 °C/s, ΔT_N increases from 2.9 °C to 5.6 °C, but Δt_N decreases from 4.8 s to 2.3 s. The increase in ΔT_N causes the increase in nucleation rate ($\dot{N}$) and the growth rate (V). There exists a linear relationship between ΔT_N and R_C, which is given by

$$\Delta T_N=1.257+1.253R_C,\ R^2=0.993 \quad (4)$$

It should be noted that the nucleation time (Δt_N) decreases when the cooling rate increases from 1.4 °C/s to 2.1 °C/s, but nearly does not decrease any more with the further increase in cooling rate to 3.5 °C/s. There are probably two stages of Δt_N separated at the cooling rate of 2.1 °C/s. In the first stage (1.4−2.1°C/s), the cooling rate is relatively low and the driving force for the nucleation is limited. So, the cooling rate has a significant influence on the undercooling time (Δt_N). In the second stage (2.1−3.5 °C/s), the cooling rate is relatively high which brings the liquid metal higher nucleation ability. Meanwhile, it also accelerates the solidification progress. So, there is no significant decrease in undercooling time (Δt_N) in the present work.

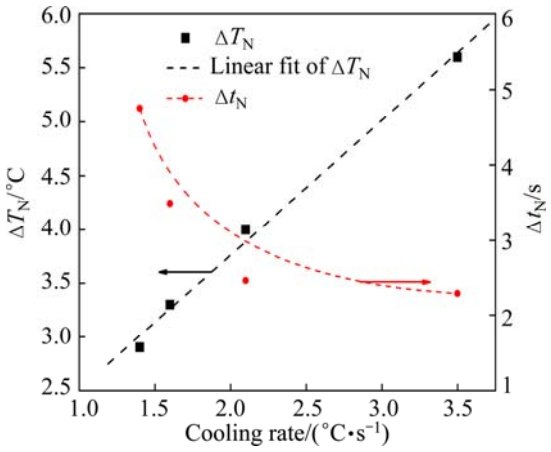

Fig. 5 Relationship between nucleation undercooling parameters (ΔT_N and Δt_N) for α-Mg phase and cooling rate

Higher cooling rate brings greater undercooling, which enhances the driving force for the nucleation and growth of the α-Mg phase. According to Kurz and David's solidification theory [26], the nucleation of the α-Mg phase has stronger effect on the grain refinement compared with the growth for the eutectic alloy. Our previous work showed that the average α-Mg grain size (d) decreased from 59 μm to 41 μm when the cooling rate increased from 1.4 °C/s to 3.5 °C/s [15]. Table 5 gives the relationship between the average α-Mg grain size (d) and undercooling parameters (ΔT_N and Δt_N) caused by different cooling rates. With the increase in the cooling rate, the average α-Mg grain size (d) decreases with the increase in the nucleation undercooling (ΔT_N), but does not decrease with the increase in the nucleation time (Δt_N). Furthermore, the polynomial relationship between d and ΔT_N is

$$d=123.65-31.375\Delta T_N+2.972\Delta T_N^{\ 2},\ R^2=0.943 \quad (5)$$

During the formation of the α-Mg phase, the total amount of nucleation (N) can be expressed as: $N=\dot{N}\cdot\Delta t_N$,

where $\dot{N}$ is the nucleation rate of the α-Mg phase, and Δt_N is the nucleation time of the α-Mg phase. It should be noted that the increased nucleation undercooling (ΔT_N) increases the driving force for the nucleation process, which enhances the nucleation rate ($\dot{N}$) directly. With the increase in cooling rate, N increases, $\dot{N}$ increases, but Δt_N decreases in the present work. With the decrease in the α-Mg grain size (d), increase in nucleation rate ($\dot{N}$) is the main reason for the grain refinement of the sand-cast GW103K alloy rather than the nucleation time (Δt_N).

Table 5 Relationship between average α-Mg grain size and nucleation undercooling (ΔT_N) and nucleation time (Δt_N) of α-Mg phase

R_C/(℃·s^{-1})	ΔT_N/℃	Δt_N/s	d/μm
1.4	2.9	4.8	59
1.6	3.4	3.5	50
2.1	4.0	2.5	43
3.5	5.6	2.3	39

The recalescence undercooling ($\Delta T_R=T_{\alpha,G}-T_{\alpha,Min}$) is a direct way to express the release process of latent heat, which can well estimate given growth during the solidification when the melt is grain refiner free [19,27]. Unlike the cooling curve of the alloy without the grain refiner, after the effective grain refiner Zr is added into the melt, the growth temperature ($T_{\alpha,G}$) is lower than the minimum temperature ($T_{\alpha,Min}$) in the present work. As a result, the recalescence undercooling ($\Delta T_R=T_{\alpha,G}-T_{\alpha,Min}$) becomes negative or even physically meaningless. The significant increase in the nuclei number caused by Zr improves the stability of the interface between the solid and the liquid, which in turn disturbs the original equilibrium of the growth process. Similar results were reported that no recalescence undercooling was observed once the grain refiner was used in as-cast Al alloys [28,29].

3.5 Solidus temperature and solidification temperature range

Figure 6 shows the effects of cooling rate on the solidus temperature (T_S) and the solidification temperature range (ΔT_S). With cooling rate increasing from 1.4 °C/s to 3.5 °C/s, the solidus temperature decreases by 5.6 °C in Fig. 6(a) and the solidification temperature range increases by 6.1 °C in Fig. 6(b). The increase in cooling rate increases the nucleation temperature ($T_{\alpha,N}$) but decreases the solidus temperature (T_S), giving an increase in the solidification temperature range (ΔT_S). Alternately, increased cooling rate decreases the solidification time (t_S), which starts at the nucleation temperature ($T_{\alpha,N}$) and ends at the solidus temperature (T_S).

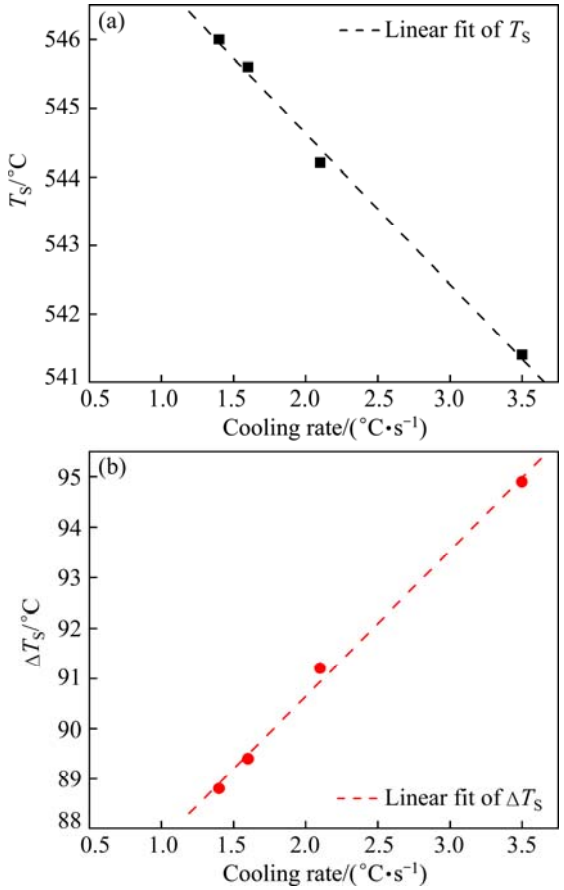

Fig. 6 Relationship between solidus temperature (T_S) and cooling rate (a), and relationship between solidification temperature range (ΔT_S) and cooling rate (b)

It should be noted that the slope value (2.193) of cooling rate in Eq. (6) is larger than that (0.701) in Eq. (1). This indicates that the cooling rate has a more significant influence on the solidus temperature (T_S) than on the nucleation temperature ($T_{\alpha,N}$), which is the actual liquid temperature in the sand-cast solidification. The linear relationships between the cooling rate and the solidus temperature (T_S) and the solidification temperature range (ΔT_S) are

$$T_S=549.02-2.193R_C,\ R^2=0.995 \quad (6)$$

$$\Delta T_S=84.853+2.894R_C,\ R^2=0.996 \quad (7)$$

3.6 Solidification parameters of eutectic reaction

Figure 7 shows the effect of the cooling rate on solidification parameters of the eutectic phases ($T_{eut,N}$, and $T_{eut,G}$). With the increase in cooling rate, the beginning temperature of the eutectic reaction ($T_{eut,N}$) increases, but the growth temperature of the eutectic phase ($T_{eut,G}$) decreases. Both $T_{eut,N}$ and $T_{eut,G}$ have linear relationships with the cooling rate. The empirical fitting functions are

$$T_{eut,N}=555.64+1.158R_C,\ R^2=0.963 \quad (8)$$

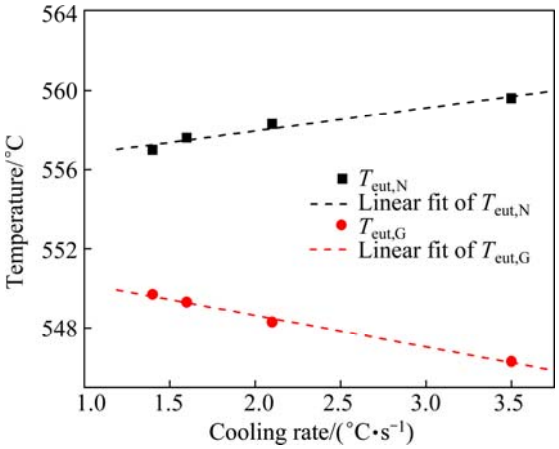

Fig. 7 Relationship between temperature parameters of eutectic phase ($T_{eut,N}$ and $T_{eut,G}$) and cooling rate

$$T_{eut,G}=551.84-1.599R_C,\ R^2=0.993 \quad (9)$$

With the increase in cooling rate, the value ($T_{eut,N}-T_{eut,G}$) increases, which brings an augmented driving force for the formation of the eutectic phase. The decreases in both $\Delta t_{eut,N}$ and $\Delta t_{eut,G}$ indicate that the value of ($\Delta t_{eut,N}+\Delta t_{eut,G}$) decreases, which means that the increased cooling rate shortens the period of the eutectic reaction. Table 4 shows that both $\Delta t_{eut,N}$ and $\Delta t_{eut,G}$ decrease with the increase in cooling rate from 1.4 °C/s to 2.1 °C/s, but do not decrease any more with further increase in cooling rate, because the cooling rate has a strong influence on the eutectic reaction as well as the solidification. On the one hand, higher cooling rate causes higher undercooling. Therefore, the eutectic reaction occurs and ends earlier. On the other hand, higher cooling rate can also accelerate the whole solidification process. As a result, the rest liquid metal does not transform into the eutectic phase but into the supersaturated solid solution.

With the cooing rate increasing from 1.4 °C/s to 3.5 °C/s, the volume fraction of the second phase increases from 17.6 % to 22.0 %, the microstructure of the eutectic phase exhibits a continuous network instead of a coarsen discontinuous network of plate-shaped particles, and a rod-like mode becomes the main morphology of the β phase instead of the lamellar structure in the eutectic phase. High cooling rate increases the nuclei density, but shortens the growth time of the α-Mg phase. On the one hand, larger number of nuclei bring about more interfaces between the solid and the liquid, which disturbs the relative stability of the original growth process of the α-Mg phase. As a result, more liquid is left for the eutectic reaction. On the other hand, the shortened growth time of the α-Mg phase implies that the volume of the liquid used for the formation of the α-Mg phase is limited. This further implies that there is more liquid available for the eutectic reaction with higher cooling rate, which causes the increase in the volume fraction of the second phase. Additionally, based on the increased nuclei number, a continuous network-shaped microstructure of the eutectic phase forms instead of the coarsening discontinuous network of plate-shaped particles. As another factor, the shortened growth time of the eutectic phase restrains the formation of the coarsening discontinuous network of plate-shaped eutectic compound when the cooling rate increases. Furthermore, high cooling rate not only leads to high undercooling for the nucleation of the α-Mg phase but also increases the driving force for the formation of the β phase in the eutectic compound. Due to the increased nuclei of the β phase caused by high undercooling, the rod-like mode becomes the main morphology of the β phase instead of the lamellar structure in the eutectic.

4 Conclusions

1) The nucleation temperature ($T_{\alpha,N}$) increases from 634.8 °C to 636.3 °C, the minimum temperature ($T_{\alpha,Min}$) decreases from 631.9 °C to 630.7 °C, the growth temperature ($T_{\alpha,G}$) decreases from 631.5 °C to 629.7 °C, the nucleation undercooling (ΔT_N) increases from 2.9 °C to 5.6 °C, the solidus temperature decreases 5.6 °C, and the solidification temperature range (ΔT_S) increases by 6.1 °C, respectively.

2) The nucleation undercooling (ΔT_N) plays a main role in the average α-Mg grain size (d) rather than the nucleation time (Δt_N). The increase in nucleation rate ($\dot{N}$) is supposed to be the main reason for the increased nuclei number (N), which directly causes the grain refinement of the studied alloy. The relationships between the modified microstructure and solidification parameters of the eutectic phase are discussed.

3) It is proved that computer aided cooling curve analysis can be used to explore the solidification behavior of the sand-cast Mg alloy. This also shows the opportunity to propose an on-line quality control algorithm to predict the effect of grain refinement and microstructure modification for the sand-cast Mg−10Gd−3Y−0.4Zr alloy solidified under the investigated conditions.

References

[1] HE Shang-min, ZENG Xiao-qin, PENG Li-ming, NIE Jian-feng, DING Wen-jiang. Precipitation in a Mg−10Gd−3Y−0.4 Zr (wt. %) alloy during isothermal ageing at 250 °C [J]. Journal of Alloys and Compounds, 2006, 421(1): 309−313.

[2] HE Shang-min, ZENG Xiao-qin, PENG Li-ming, NIE Jian-feng, DING Wen-jiang. Microstructure and strengthening mechanism of high strength Mg−10Gd−2Y−0.5Zr alloy [J]. Journal of Alloys and Compounds, 2007, 427(1): 316−323.

[3] CHEN Xian-hua, HUANG Xiao-wang, PAN Fu-sheng, TANG Ai-tao, WANG Jing-feng, ZHANG Ding-fei. Effects of heat treatment on microstructure and mechanical properties of ZK60 Mg alloy [J]. Transactions of Nonferrous Metals Society of China, 2011, 21(4): 754−760.

[4] HUANG Ming-li, LI Hong-xiao, DING Hua, BAO Li, MA Xiao-bin, HAO Shi-ming. Intermetallics and phase relations of Mg−Zn−Ce alloys at 400 °C [J]. Transactions of Nonferrous Metals Society of China, 2012, 22(3): 39−545.

[5] ZHANG Xue-feng, WU Guo-hua, LIU Wen-cai, DING Wen-jiang. Low temperature mechanical properties of as-extruded Mg−10Gd−3Y−0.5Zr magnesium alloy [J]. Transactions of Nonferrous Metals Society of China, 2012, 22(12): 2883−2890.

[6] LI Ji-lin, CHEN Rong-shi, KE Wei. Microstructure and mechanical properties of Mg−Gd−Y−Zr alloy cast by metal mould and lost foam casting [J]. Transactions of Nonferrous Metals Society of China, 2011, 21(4): 761−766.

[7] ZHANG Kui, LI Xing-gang, LI Yong-jun, MA Ming-long. Effect of Gd content on microstructure and mechanical properties of Mg−Y−RE−Zr alloys [J]. Transactions of Nonferrous Metals Society of China, 2011, 18(S): s12−s16.

[8] CAO Liang, LIU Wen-cai, LI Zhong-quan, WU Guo-hua, XIAO Lü, WANG Shao-hua, DING Wen-jiang. Effect of heat treatment on microstructures and mechanical properties of sand-cast Mg−10Gd−3Y−0.5Zr magnesium alloy [J]. Transactions of Nonferrous Metals Society of China, 2014, 24(3): 611−618.

[9] GAO Lei, CHEN Rong-shan, HAN En-Hou. Enhancement of ductility in high strength Mg−Gd−Y−Zr alloy [J]. Transactions of Nonferrous Metals Society of China, 2011, 21(4): 863−868.

[10] SUN Ming, WU Guo-hua, WANG Wei, DING Wen-jiang. Effect of Zr on the microstructure, mechanical properties and corrosion resistance of Mg−10Gd−3Y magnesium alloy [J]. Materials Science and Engineering A, 2009, 523(1): 145−151.

[11] HONMA T, OHKUBO T, KAMADO S, HONO K. Effect of Zn additions on the age-hardening of Mg−2.0Gd−1.2Y−0.2Zr alloys [J]. Acta Materialia, 2007, 55(12): 4137−4150.

[12] WU Guo-hua, ZHANG Yang, LIU Wen-cai, DING Wen-jiang. Effects of rotating gas bubble stirring treatment on the microstructures of semi-solid AZ91−2Ca alloy [J]. Journal of Magnesium and Alloys, 2013, 1(3): 217−223.

[13] LIU Zhi-jie, WU Guo-hua, LIU Wen-cai, PANG Song, DING Wen-jiang. Effects of heat treatment on microstructures and mechanical properties of sand-cast Mg−4Y−2Nd−1Gd−0.4Zr magnesium alloy [J]. Transactions of Nonferrous Metals Society of China, 2012, 22(7): 1540−1548.

[14] LIU Zhi-jie, WU Guo-hua, LIU Wen-cai, PANG Song, DING Wen-jiang. Microstructure, mechanical properties and fracture behavior of peak-aged Mg−4Y−2Nd−1Gd alloys under different aging conditions [J]. Materials Science and Engineering A, 2013, 561: 303−311.

[15] PANG Song, WU Guo-hua, LIU Wen-cai, SUN Ming, ZHANG Yang, LIU Zhi-jie, DING Wen-jiang. Effect of cooling rate on the microstructure and mechanical properties of sand-casting Mg−10Gd−3Y−0.5Zr magnesium alloy [J]. Materials Science and Engineering A, 2013, 562(1): 152−160.

[16] ROHATGI P K, DAOUD A, SCHULTZ B F, PURI T. Microstructure and mechanical behavior of die casting AZ91D-Fly ash cenosphere composites [J]. Composites Part A: Apply Science Manufacturing, 2009, 40(6): 883−896.

[17] CACERES C H, DAVIDSON C J, GRIFFITHS J R, NEWTON C L. Effects of solidification rate and ageing on the microstructure and mechanical properties of AZ91 alloy [J]. Materials Science and Engineering A, 2002, 325(1): 344−355.

[18] EMADI D, WHITING L V, NAFISI S, GHOMASHCHI R. Applications of thermal analysis in quality control of solidification processes [J]. Journal of Thermal Analysis and Calorimetry, 2005, 81(1): 235−242.

[19] XU Jun-feng, LIU Feng, XU Xiao-long, CHEN Yu-zeng. Determination of solid fraction from cooling curve [J]. Metallurgical and Materials Transactions A, 2012, 43(4): 1268−1276.

[20] MACKAY R I, DJURDJEVIC M B, SOKOLOWSKI J H. Effect of cooling rate on fraction solid of metallurgical reactions in 319 alloy [J]. Transactions of the American Foundrymen's Society, 2000, 108: 521−530.

[21] FARAHANY S, OURDJINI A, IDRIS M H. The usage of computer-aided cooling curve thermal analysis to optimise eutectic refiner and modifier in Al−Si alloys [J]. Journal of Thermal Analysis and Calorimetry, 2012, 109(1): 105−111.

[22] APARICIO R, BARRERA G, TRAPAGA G, RAMIREZ-ARGAEZ M, GONZALEZ-RIVERA C. Solidification kinetics of a near eutectic Al−Si alloy, unmodified and modified with Sr [J]. Metals and Materials International, 2013, 19(4): 707−715.

[23] FARAHANY S, OURDJINI A, IDRIS M H, SHABESTARI S G. Evaluation of the effect of Bi, Sb, Sr and cooling condition on eutectic phases in an Al−Si−Cu Alloy (ADC12) by in-situ thermal analysis [J]. Thermochimica Acta, 2013, 559(10): 59−68.

[24] GOURLAY C M, DAHLE A K. Dilatant shear bands in solidifying metals [J]. Nature, 2007, 445(4): 70−73.

[25] YAMAGATA H, KURITA H, ANIOLEK M, KASPRZAK W, SOKOLOWSKI J H. Thermal and metallographic characteristics of the Al−20%Si high-pressure die-casting alloy for monolithic cylinder blocks [J]. Journal of Materials Processing Technology, 2008, 199(1−3): 84−90.

[26] WILFRIED K, FISHER D J. Fundamentals of solidification [M]. Aedermannsdorf, Switzerland: Trans Tech Publications Ltd, 1986.

[27] HEINE R W, LOPER C R, ROSENTHAL P C. Principles of metal casting [M]. New York: McGraw Hill, 1978.

[28] SHABESTARI S G, GHODRAT S. Assessment of modification and formation of intermetallic compounds in aluminum alloy using thermal analysis [J]. Materials Science and Engineering A, 2007, 467(1): 150−158.

[29] SHABESTARI S G, MALEKAN M. Assessment of the effect of grain refinement on the solidification characteristics of 319 aluminum alloy using thermal analysis [J]. Journal of Alloys and Compounds, 2010, 492(1): 134−142.

冷却速率对砂型铸造 Mg−10Gd−3Y−0.4Zr 合金凝固行为的影响

庞 松[1,2]，吴国华[1]，刘文才[1]，张 亮[1]，张 扬[1]，Hans CONRAD[2]，丁文江[1]

1. 上海交通大学 轻合金精密成型国家工程研究中心与金属基复合材料国家重点实验室，上海 200240；
2. Materials Science and Engineering Department, North Carolina State University, Raleigh, NC 27695-7907, USA

摘 要：采用计算机辅助冷却曲线分析技术研究砂型铸造过程中冷却速率(1.4~3.5 °C/s)对 Mg−10Gd−3Y−0.4Zr 合金凝固行为的影响。结果表明：随着冷却速率的提高，起始形核温度($T_{\alpha,N}$)由 634.8 °C 升至 636.3 °C，再辉前最低温度($T_{\alpha,Min}$)由 631.9 °C 降至 630.7 °C，形核过冷度(ΔT_N)由 2.9 °C 升至 5.6 °C，共晶反应起始温度($T_{eut,N}$)上升，固相线温度(T_S)由 546.0 °C 降至 541.4 °C，凝固温度区间(ΔT_S)增加 6.1 °C。形核速率($\dot{N}$)的增加引起晶核数量的增加，从而降低 α-Mg 的平均晶粒粒径。相对于形核时间(Δt_N)，形核过冷度(ΔT_N)对 α-Mg 平均晶粒粒径的影响更大。温度增加值($T_{eut,N}-T_{eut,G}$)与缩短的反应时间改变共晶反应进程，并且影响第二相的含量以及形貌。

关键词：Mg−10Gd−3Y−0.4Zr；砂型铸造；冷却速率；热分析；凝固行为

(Edited by Yun-bin HE)